# There can be no '$CO_2$ Signal' in the Global Mean Temperature Record


## Roy Clark PhD

Thousand Oaks, CA 91360

January 14, 2023

**Table of Contents**

**Summary**

When the time dependent flux terms are used in a thermal engineering analysis of the surface temperature, it becomes clear that there can be no '$CO_2$ signal' in the global mean temperature record. The temperature changes produced by the measured 140 parts per million (ppm) increase the in atmospheric $CO_2$ concentration since the start of the Industrial Revolution are too small to measure in the normal temperature variations found in the climate system. In particular, the quasi-periodic oscillations in ocean surface temperature provide a natural 'noise floor' for the climate system. This is the dominant term in the temperature record. The claim that the global mean temperature record can be explained by the radiative forcings and feedbacks used in the 'equilibrium' climate models is pseudoscientific nonsense.

**Introduction**

The root cause of the errors in the climate models is the equilibrium assumption. Starting in the nineteenth century, the time dependence of the flux terms was replaced by equilibrium average values. Physical reality was abandoned in favor of mathematical simplicity. This led to the introduction of the 'equilibrium air column' first used by Arrhenius [1896]. This approach was incorporated into the one dimensional radiative convective (1-D RC) model described by Manabe and Wetherald (M&W) [1967]. When the $CO_2$ concentration is increased in this model, the simplifying assumptions used by M&W had to create global warming as a mathematical artifact in the model output. Their assumption of a prescribed relative humidity distribution also created the 'water vapor feedback' that amplified the $CO_2$ warming artifact. M&W then incorporated their 1967 model into a 'highly simplified' global circulation model (GCM). Here, the 1967 model artifacts were incorporated into each unit cell of the GCM. This model also created a 'hot spot' in the troposphere at lower latitudes [M&W, 1975].

The 1-D RC model artifacts were later used by Ramanathan [1974] to claim global warming by chlorofluorocarbons. This gradually led to the concept of radiative forcing [Ramaswamy et al 2019]. The 1-D RC model artifacts were also used by the climate modeling group at NASA Goddard to create global warming from a variety of 'greenhouse gases', starting with the work of Wang and Domoto [1974] and Wang et al [1976]. Additional modeling assumptions were introduced by the Goddard group in 1981. These included a 'slab' ocean model, the $CO_2$ doubling ritual for the 1-D RC model and the claim that the 1-D RC modeling artifacts could be used to simulate the global mean temperature record [Hansen et al, 1981]. The only change in the basic modeling assumptions since 1981 was the addition of 'efficacies' to the radiative forcings by Hansen's group [2005]. As computer technology has improved, the climate models have become more complex, but the underlying equilibrium assumption has not changed. The mathematical warming artifacts are 'tuned' by the climate modelers using a contrived set of pseudoscientific radiative forcings and feedbacks to make the climate model output appear to match the global mean temperature record.

The introduction to Chapter 7 of the Working Group 1 Report in the latest UN Intergovernmental Panel on Climate Change (IPCC) Climate Assessment, AR6, WG1 '*The Earth's energy budget, climate feedbacks, and climate sensitivity*' [IPCC, 2021] starts:

> This chapter assesses the present state of knowledge of Earth's energy budget, that is, the main flows of energy into and out of the Earth system, and how these energy flows govern the climate response to a radiative forcing. Changes in atmospheric composition and land use, like those caused by anthropogenic greenhouse gas emissions and emissions of aerosols and their precursors, affect climate through perturbations to Earth's top-of-atmosphere energy budget. The effective radiative forcings (ERFs) quantify these perturbations, including any consequent adjustment to the climate system (but excluding surface temperature response). How the climate system responds to a given forcing is determined by climate feedbacks associated with physical, biogeophysical and biogeochemical processes. These feedback processes are assessed, as are useful measures of global climate response, namely equilibrium climate sensitivity (ECS) and the transient climate response (TCR).

A more concise summary was provided by Knutti and Hegerl [2008]:

> When the radiation balance of the Earth is perturbed, the global surface temperature will warm and adjust to a new equilibrium state.

When the time dependent climate energy transfer processes that determine the surface temperature are examined in more detail it becomes clear that:

1) An infrared 'radiative forcing' does not change the 'energy balance' of the earth.
2) An infrared 'radiative forcing' does not produce a measurable increase in ocean surface temperature.
3) An infrared 'radiative forcing' does not produce a measurable increase in land surface temperature.
4) There can be no 'climate sensitivity' to $CO_2$.

This also means that increases in extreme weather events cannot be 'attributed' to $CO_2$ and that the 1.5 or 2 °C limit incorporated into the Paris Climate Accord is pseudoscientific nonsense.

In addition, the climate models require the solution of very large numbers of coupled non-linear equations. The errors associated with this type of modeling grow over time. These are known as Lorenz instabilities [Lorenz, 1963; 1973]. There is no reason to expect these climate models to have any predictive capabilities over the time scales involved in climate studies.

The required thermal engineering analysis may be defined as follows:

Since the start of the Industrial Revolution about 200 years ago, the atmospheric concentration of $CO_2$ has increased by approximately 140 parts per million (ppm), from 280 to 420 ppm [Keeling, 2022]. This has produced a decrease near 2 W $m^{-2}$ in the longwave IR (LWIR) flux emitted to

space at the top of the atmosphere (TOA) within the spectral range of the $CO_2$ emission bands. There has also been a similar increase in the downward LWIR flux from the lower troposphere to the surface [Harde, 2017]. For a '$CO_2$ doubling' from 280 to 560 ppm, the decrease in outgoing longwave radiation (OLR) is estimated to be 3.7 W $m^{-2}$ [IPCC, 2013]. At present, the average annual increase in $CO_2$ concentration is near 2.4 ppm. This produces an increase in the downward LWIR flux to the surface of approximately 0.034 W $m^{-2}$ per year. The changes in $CO_2$ concentration are shown in Figure 1a and the changes in total flux are shown in Figure 1b. More detailed calculations of the change in flux at TOA produced by increases in the atmospheric concentration of $H_2O$, $CO_2$, $O_3$, $N_2O$ and $CH_4$ have been provided by Wijngaarden and Happer [2022].

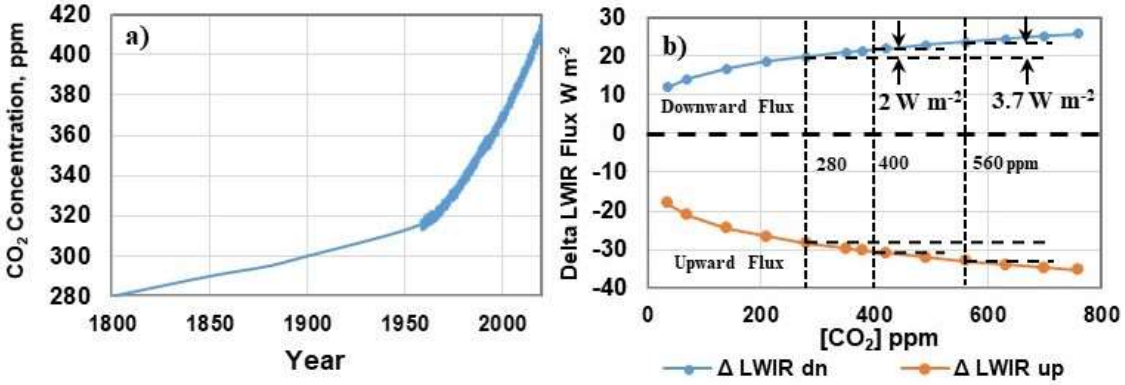


**Figure 1: a) the measured increase in atmospheric $CO_2$ concentration from 1800 (Keeling curve) and b) calculated changes in atmospheric LWIR flux produced by an increase in atmospheric $CO_2$ concentration from 0 to 760 ppm.**

In a non-equilibrium system, a change in flux produces a change in the rate of heating or cooling of a thermal reservoir. A change in temperature has to be determined by taking the change in heat content or enthalpy of the thermal reservoir of interest over a given time period and dividing this by the local heat capacity. In addition to the LWIR flux, the solar heating, the evapotranspiration (moist convection) and the subsurface thermal transport are all coupled to the surface thermal reservoir and must be included in the analysis of the surface temperature. The energy transfer processes at the land-air and ocean-air interfaces are different and have to be considered separately.

Convection is also a mass transport process that is coupled to the gravitational potential and the rotation of the earth. These interactions result in the formation of the Hadley, Ferrell and polar cell convective structure, the trade winds and the ocean gyre circulation. This is the source of the earth's weather patterns. In the troposphere, vertical motion changes the temperature of an air parcel by air compression/expansion. This process is fully coupled to the air parcel cooling produced by the net LWIR emission.

**Radiative Forcing by $CO_2$ does not Change the Radiation Balance of the Earth**

When the atmospheric concentration of a greenhouse gas is increased, there is a decrease in the LWIR flux emitted to space at TOA, within the spectral region of the absorption/emission band

specific to each greenhouse gas considered [Wijngaarden and Happer, 2022]. A change in flux at TOA is considered to be 'radiative forcing' that changes the radiation balance of the earth. Other radiative forcings, such as changes in aerosol concentration may increase the reflected solar flux at TOA. The standard climate 'perturbation' or radiative forcing used to compare the climate models is a doubling of the $CO_2$ concentration from 280 to 560 ppm. The increase in global mean surface temperature created by a '$CO_2$ doubling' in a climate model is called the climate sensitivity. There is both an equilibrium climate sensitivity (ECS) and a transient climate response (TCR).

Most of the initial decrease in LWIR emission for a $CO_2$ doubling occurs in the P and R branches of the $\nu_2$ $CO_2$ band near 640 and 700 $cm^{-1}$. There is also a slight decrease in the weaker emission by the $CO_2$ overtone bands near 950 and 1050 $cm^{-1}$. However, an LWIR 'radiative forcing' does not magically appear at TOA. It is produced by small changes in emission at many different levels in the atmosphere. The emission from each level is modified by the absorption and emission of the levels above. In order to understand the atmospheric heating effects of a '$CO_2$ doubling', the change in net LWIR flux has to be calculated at each level in the atmosphere and converted to a change in the rate of cooling by dividing by the heat capacity of the local air parcel. The total (10 to 3250 $cm^{-1}$) and spectral band average LWIR cooling rates for a tropical atmosphere are shown in Figure 2a [Feldman et al, 2017]. The LWIR cooling rate for most of the troposphere at low latitudes is in the range 2 to 2.5 K per day. The change in the rate of LWIR cooling in the troposphere produced by a doubling of the $CO_2$ concentration is shown in Figure 2b [Iacono et al, 2008]. The maximum change is +0.08 K per day. At a lapse rate of -6.5 K $km^{-1}$, this daily change in temperature is equivalent to riding an elevator down four floors.

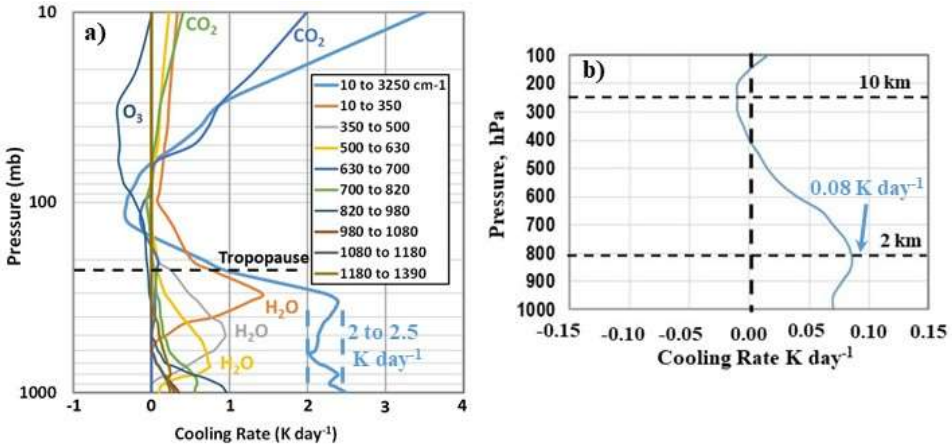


**Figure 2: a) Total (10 to 3250 $cm^{-1}$) and band-averaged IR cooling rate profiles for the Tropical Model Atmosphere on a log-pressure scale. b) Tropospheric heating rates produced by a $CO_2$ 'doubling' from 287 to 574 ppm at mid latitude.**

The atmospheric LWIR flux consists of IR emission and absorption from many overlapping lines [Wijngaarden, and Happer, 2022]. Each line is a specific transition between two molecular rotation-vibration states. The lines are broadened by molecular collisions. Near the surface within the main absorption emission bands, the lines overlap and merge into a quasi-continuum. At higher altitudes, these lines become narrower as the temperature and pressure decrease. Some of the

upward LWIR flux can pass through the gaps between these narrower lines above and continue to space without additional absorption/emission. The downward flux is absorbed by the broader lines below. This is illustrated schematically in Figure 3a for a single line and in Figure 3b for a group of lines in the 590 to 600 $cm^{-1}$ region. Almost all of the downward LWIR flux that reaches the surface originates from within the first 2 km layer of the troposphere. Approximately half of this downward flux originates from the first 100 m layer. This is shown in Figure 3c [Clark, 2013]. The downward LWIR flux to the surface is therefore decoupled from the LWIR emission to space.

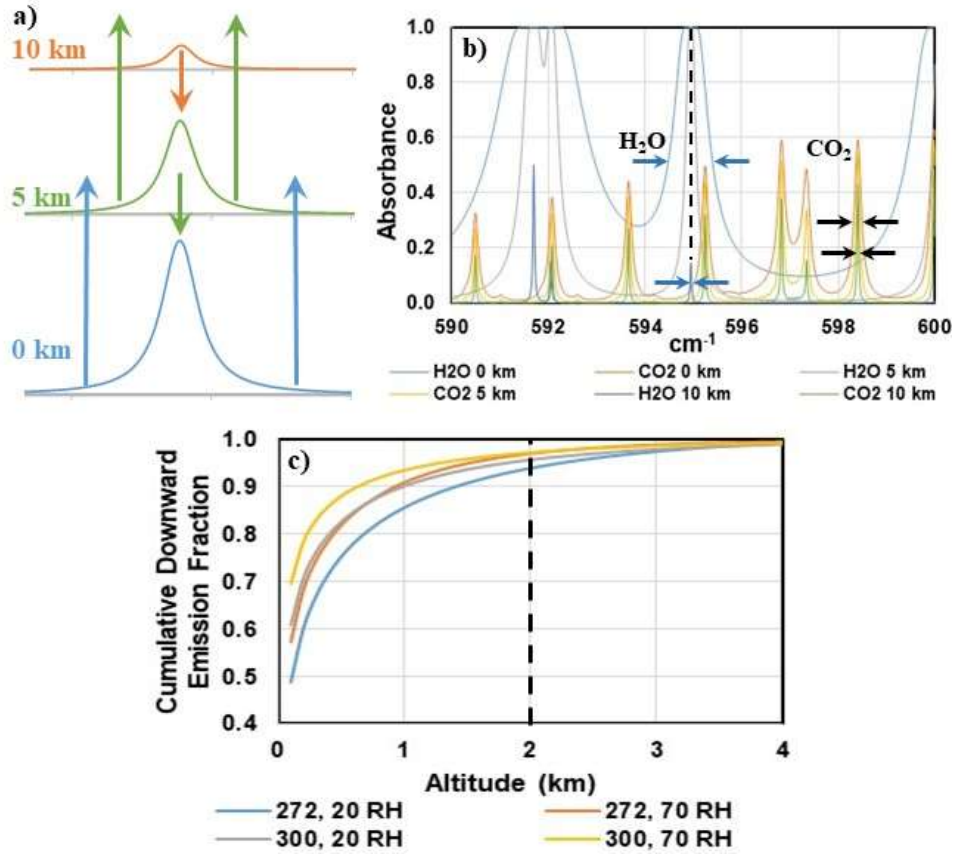


**Figure 3: a) Transition from absorption-emission to free photon flux as the linewidth decreases with altitude. Single $H_2O$ line near 231 $cm^{-1}$. b) Linewidths for $H_2O$ and $CO_2$ lines in the 590 to 600 $cm^{-1}$ spectral region for altitudes of 0, 5 and 10 km. c) Cumulative fraction of the downward flux at the surface vs. altitude for surface temperatures of 272 and 300 K, each with 20 and 70% relative humidity (RH). Almost all of the downward flux reaching the surface originates from within the first 2 km layer. This is the location of the lower tropospheric reservoir.**

The downward LWIR flux from the lower troposphere to the surface establishes a partial LWIR exchange energy with the upward LWIR flux emitted by the surface. When the surface and surface air layer are at similar temperatures, IR photons are exchanged without any significant transfer of thermal energy. The net LWIR cooling flux (upward minus downward LWIR flux) at the surface is limited to the emission into the LWIR atmospheric transmission window. This LWIR flux is insufficient to dissipate the absorbed solar insolation. The surface warms up so that the excess solar heat is removed by moist convection. This drives the tropospheric heat engine. The net

cooling flux changes with temperature, humidity and cloud cover. In particular, clouds are close to blackbody emitters. The downward LWIR flux from the cloud base 'fills in' the atmospheric LWIR transmission window. This is illustrated in Figure 4. When the surface is warmer than the air layer above, the excess upward LWIR flux emitted by the surface outside of the LWIR transmission window is absorbed in the lower troposphere and can increase the convection [Clark and Rorsch, 2023; Clark, 2013]. The ocean-air and the land-air interfaces have different energy transfer properties and have to be analyzed separately.

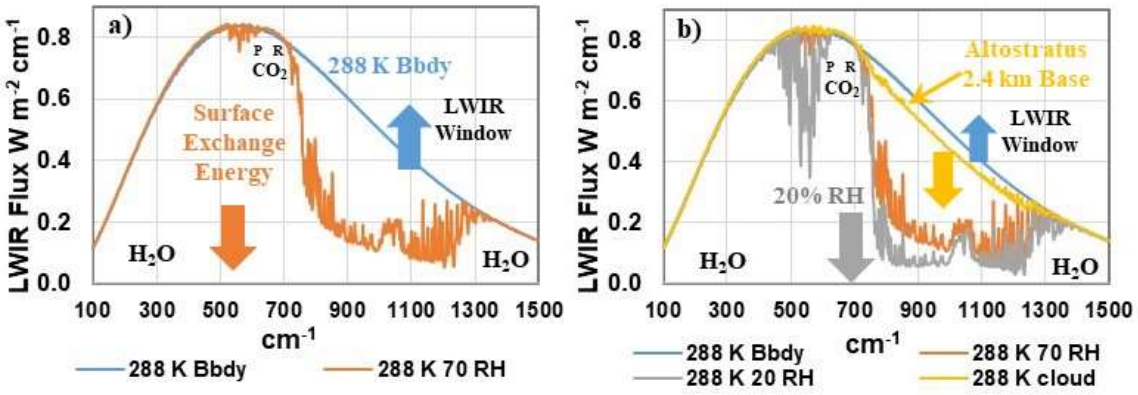


**Figure 4: The surface exchange energy for surface and air temperatures of 288 K. a) Blackbody surface emission and downward LWIR flux for a relative humidity of 70% and $CO_2$ concentration of 400 ppm. The $H_2O$ and $CO_2$ bands are indicated. b) Same as a) with the downward emission for 20% RH and for altostratus cloud cover with a 2.5 km cloud base added. MODTRAN calculations, 100 to 1500 $cm^{-1}$ spectral range, 2 $cm^{-1}$ spectral resolution [MODTRAN, 2021].**

Figure 5a illustrates the energy transfer processes for an air parcel in the troposphere (within the plane parallel atmosphere approximation). The air parcel is emitting LWIR radiation upwards and downwards at the local temperature. It is also absorbing part of the upward LWIR flux from below and the downward LWIR flux from above. The air parcel is also in a turbulent convective flow field. Vertical motion changes the temperature of the air parcel at the local lapse rate. Figure 5b illustrates the dissipation of the radiative forcing in the troposphere produced by an increase in the atmospheric $CO_2$ concentration. The small amount of heat that is produced at each level is coupled to the local air parcel and dissipated as wideband LWIR emission, mainly by the water bands. Any change in temperature is too small to measure.

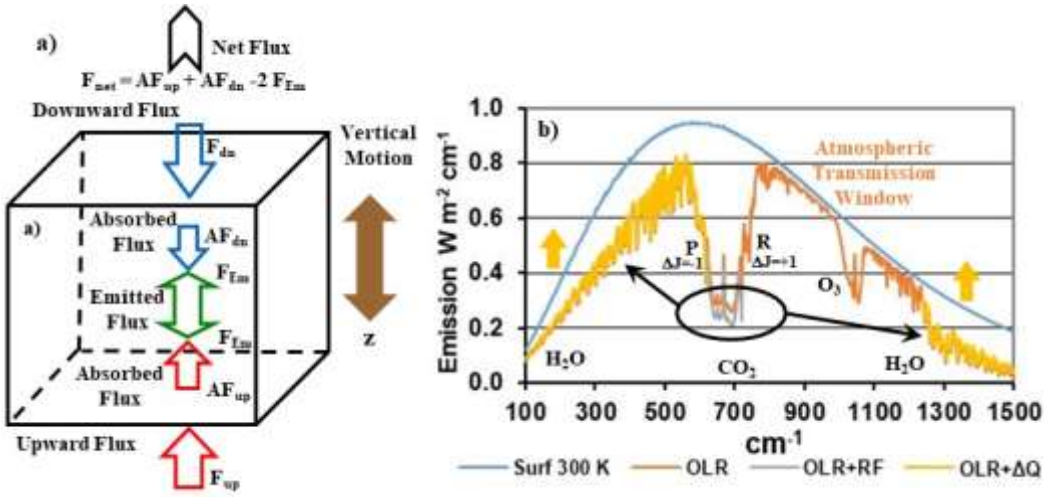


**Figure 5: a) The energy transfer processes for a local tropospheric air parcel (in a plane-parallel atmosphere) and b) the dissipation of the absorbed heat from a '$CO_2$ doubling' by the normal tropospheric energy transfer processes (schematic). The wavelength specific increase in absorption in the $CO_2$ P and R bands is dissipated as small changes in broadband LWIR emission and gravitational potential energy.**

Figure 6 shows the vertical velocity profile up to 2 km altitude in the turbulent surface boundary layer. This is from Doppler heterodyne LIDAR measurements recorded over 10 hours at the École Polytechnique, south of Paris, July 10th 2005 [Gibert et al, 2007]. The change in vertical velocity is ±2 m s$^{-1}$. This is sufficient to overwhelm any changes in cooling from a '$CO_2$ doubling' as shown in Figure 2b. The LWIR radiative forcings produced by the increase in atmospheric concentration of 'greenhouse gases' cannot change the energy balance of the earth.

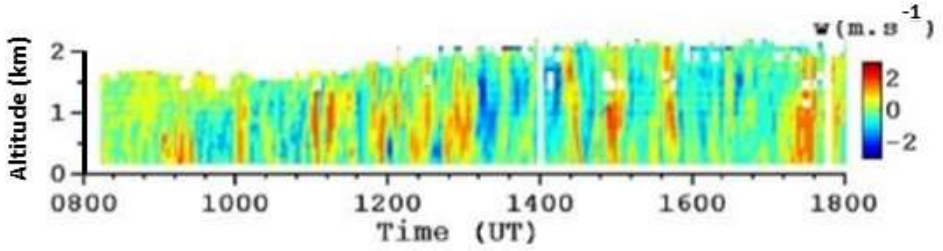


**Figure 6: Vertical velocity profile in the turbulent boundary layer recorded over 10 hours at the École Polytechnique, south of Paris, July 10th 2005 using Doppler heterodyne LIDAR.**

## An Increase in $CO_2$ Concentration Cannot Produce a Measurable Change in Ocean Surface Temperature

Over the oceans, the surface is almost transparent to the solar flux. The diurnal temperature rise is small and the bulk ocean temperature increases until the water vapor pressure at the surface is sufficient for the excess absorbed solar heat to be removed by wind driven evaporation. The sensible heat flux is usually small, less than 10 W m$^{-2}$. The penetration depth of the LWIR flux into the ocean surface is less than 100 micron. This is illustrated in Figure 7 [Hale and Querry, 1973]. The LWIR flux and the wind driven evaporation are coupled together at the surface and should not be analyzed separately. The cooler water produced at the surface sinks and is replaced

by warmer water from the bulk ocean below. This allows the evaporation to continue at night. Figure 8 shows the long term zonal average sensitivity of the latent heat flux to the wind speed. This is calculated from the long term zonal average ocean latent heat flux and wind speed data given by Yu et al [2008]. Over the ±30° latitude bands, the sensitivity is at least 15 W $m^{-2}$/m $s^{-1}$. As shown above in Figure 1b, the increase in downward LWIR flux to the surface produced by the observed 140 ppm increase in atmospheric $CO_2$ concentration is approximately 2 W $m^{-2}$. Within the ±30° latitude bands, this is dissipated by an increase in wind speed near 13 cm $s^{-1}$. For comparison, the long term 1σ variation in wind speed along the equator, measured by the TRITON buoy network is near 2 m $s^{-1}$ [Clark and Rörsch, 2023]. The average annual increase in atmospheric $CO_2$ concentration at present is near 2.4 ppm. This corresponds to an annual increase of 0.034 W $m^{-2}$ in the downward LWIR flux to the surface which is dissipated by an increase in wind speed near 2 millimeters per second. Any change in ocean temperature produced by the current annual increase in the atmospheric $CO_2$ concentration is therefore too small to measure.

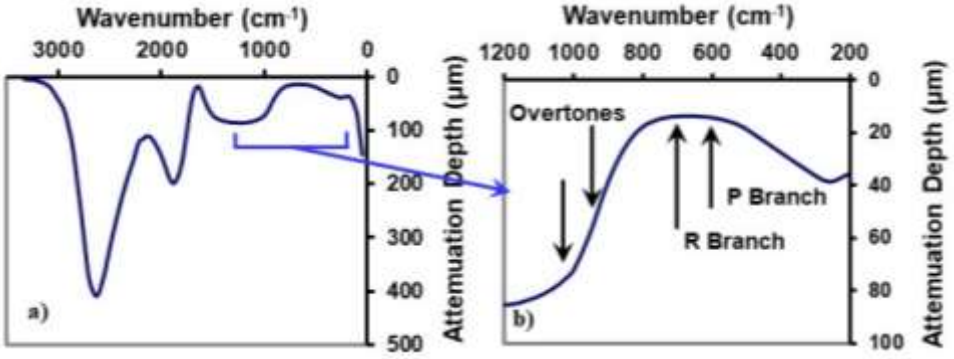


**Figure 7: The penetration depth (99% absorption) of the LWIR flux into water a) below 3300 $cm^{-1}$ and b) 1200 to 200 $cm^{-1}$. The locations of the main $CO_2$ absorption bands and the overtones are indicated.**

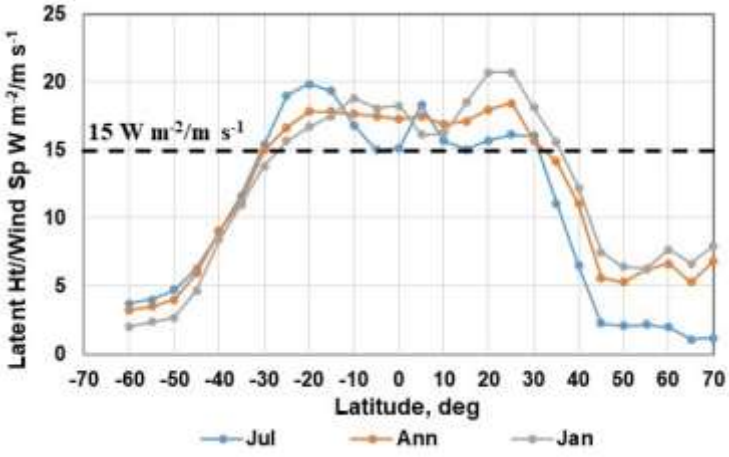


**Figure 8: The sensitivity of the ocean latent heat flux to the wind speed.**

## The Increase in $CO_2$ Concentration Cannot Produce a Measurable Change in Land Surface Temperature

Over land, all of the flux terms are absorbed by a thin surface layer. The surface temperature initially increases after sunrise as the solar flux is absorbed. This establishes a thermal gradient with both the cooler air above and the subsurface ground layers below. The surface-air gradient drives the evapotranspiration and the subsurface gradient conducts heat below the surface during the first part of the day after sunrise. Later in the day, as the surface cools, the subsurface gradient reverses and the stored heat is returned to the surface. As the land and air temperatures equalize in the evening, the convection stops and the surface cools more slowly by net LWIR emission. This convection transition temperature is reset each day by the local weather system passing through. Almost all of the absorbed solar heat is dissipated within the same diurnal cycle. The heat transfer is localized. The diurnal temperature change is limited to a shallow depth, typically 0.5 to 2 m, and the seasonal temperature variations may extend to 5 m below the surface [Clark and Rörsch, 2023; Clark, 2013]. There are also characteristic phase shifts or time delays between the peak solar flux and the temperature response. These are not a new discovery. The subsurface seasonal phase shift was described by Fourier in 1824 [Fourier, 1824]. The soil temperatures at depths from 0.5 to 80 cm and the 2 m air temperature recorded at a monitoring site at O'Neill, Neb., August 13, 1953 are shown in Figure 9 [Lettau and Davidson 1957]. The surface temperature phase shift, δt, is indicated. Below the surface, the temperature rise decreases and the phase shift increases with the depth. At the surface, the temperature rise is 22 °C. The surface air temperature rise at 1.5 m above the surface is 15 °C. There is almost no measurable diurnal phase shift below 50 cm depth.

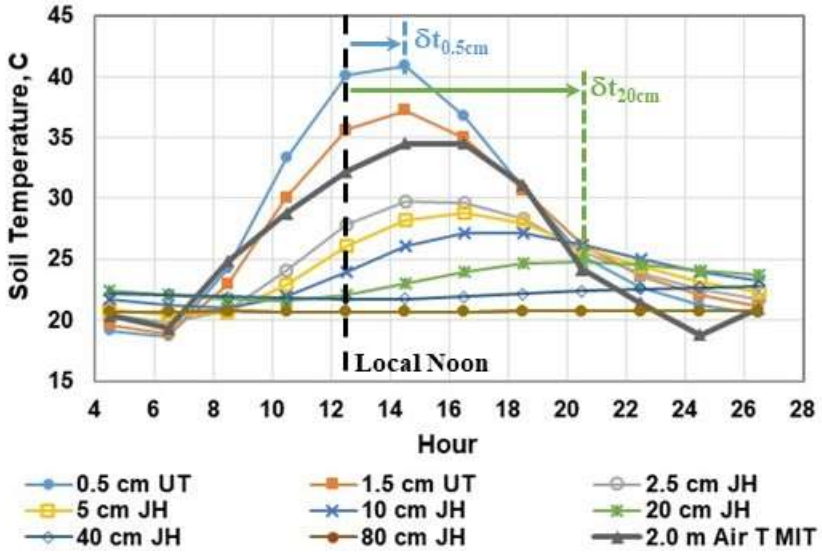


**Figure 9: 2 m air temperature and subsurface temperatures measured at O'Neill, Neb., August 13, 1953.**

The various flux terms interact with the surface and change the temperature at the land-air interface. However, the weather station temperature is the meteorological surface air temperature (MSAT) measured in a ventilated enclosure located at eye level, 1.5 to 2 m above the ground [Oke,

2006]. In general, the minimum MSAT and the minimum surface temperature are similar, but the maximum surface temperature is larger than the maximum MSAT. The minimum and maximum temperatures are determined by different energy transfer processes. The minimum temperature is reset each day by the bulk surface air temperature of the local weather system passing through. The maximum surface temperature is set by the balance between the solar heating, the combined net LWIR flux and evapotranspiration (moist convection) and the subsurface thermal transport. The maximum MSAT is determined by the mixing of the warm air rising from the surface with the cooler air at the level of the MSAT thermometer. The important physical variables in the weather station temperature data are therefore the minimum MSAT and the delta T or difference between the maximum and minimum MSAT. The average MSAT, $(T_{max} + T_{min})/2$, has little useful meaning.

To illustrate the normal variation in the MSAT record, the 1981 to 2010 30 year daily climate averages for the O'Neill, Neb. weather station #256290 are shown in Figure 10 [WRCC, 2022]. The 1σ standard deviations and the ΔT ($T_{max}$ - $T_{min}$) values are also shown. There is a phase shift of approximately 30 days between the peak solar flux at summer solstice, day 172 and the peak seasonal temperature response. In addition, the ΔT values remain within the approximate range 13.4 ±2 °C for the entire year while the temperature variation is ±10 °C. The 1σ temperature standard deviations increase from approximately 4 °C in summer to 8 °C in winter.

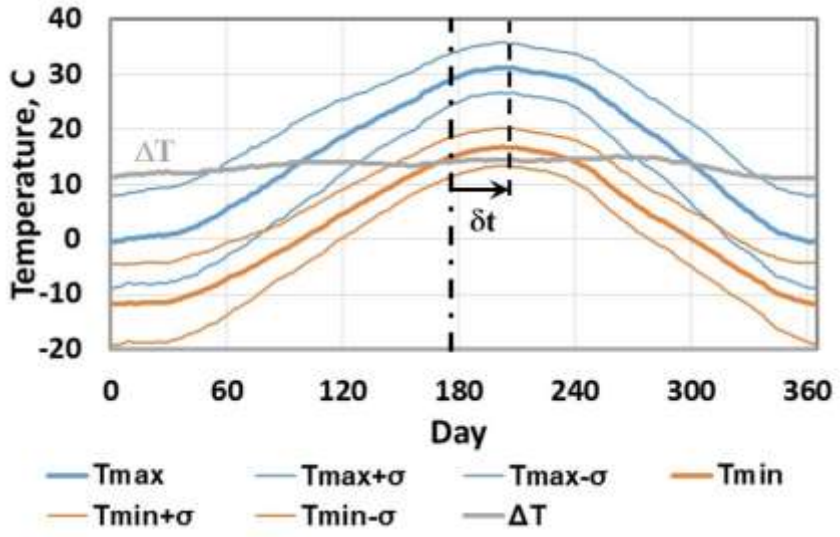


**Figure 10: 1981-2010 daily climate averages for O'Neill, Neb., Station #256290. The 1σ standard deviations and the ΔT ($T_{max}$ -$T_{min}$) are also shown. The seasonal phase shift, δt is indicated.**

A simple thermal engineering model of the surface and air temperatures recorded in 2008 at the 'Grasslands' site, an advanced AmeriFlux monitoring station located in Limestone Canyon Regional Park, near Irvine, S. California was used to evaluate the effect of an increase in $CO_2$ concentration on land temperatures [Clark and Rörsch, 2023; Clark, 2013]. In this case, for a doubling of the $CO_2$ concentration from 280 to 560 ppm, the increase in MSAT was approximately 0.1 C. This is too small to measure in the normal day to day variations in the convection transition

temperature. In addition, the diurnal and seasonal phase shifts demonstrate that the surface thermal reservoir is not in thermal equilibrium.

**There can be no climate sensitivity to $CO_2$**

When the climate anomaly record, such as the HadCRUT4 data set is evaluated, the dominant term is found to be the Atlantic Multi-decadal Oscillation (AMO) [HadCRUT4, 2022]. This is illustrated in Figure 11a. The AMO is a long term quasi-periodic oscillation in the surface temperature of the N. Atlantic Ocean from 0° to 60° N [AMO, 2022]. Superimposed on the oscillation is a linear increase in temperature related to the recovery from the Little Ice Age (LIA) or Maunder minimum [Akasofu, 2010]. The linear equation for the slope and the least squares fit to the oscillation are shown on Figure 11a. Before 1970, the AMO and HadCRUT4 track quite closely. This includes both the long period oscillation and short term fluctuations. There is an offset that starts near 1970 with HadCRUT4 approximately 0.3 ℃ higher than the AMO. The short term fluctuations are still similar. The correlation coefficient between the two data sets is 0.8. The influence of the AMO extends over large areas of N. America, Western Europe and parts of Africa. The weather systems that form over the oceans and move overland couple the ocean surface temperature to the weather station data through the diurnal convection transition temperature [Clark and Rörsch, 2023]. The contributions of the other ocean oscillations to the global temperature anomaly are smaller. The IOD and the PDO are dipoles that tend to cancel and the ENSO is limited to a relatively small area of the tropical Pacific Ocean. However, small surface temperature variations in the tropical oceans have a major impact on ocean evaporation and rainfall. Figure 11b shows a tree ring construction of the AMO from 1567 [Gray, 2004, Gray.NOAA, 2021]. The modern instrument record is also indicated in green. None of the temperature changes related to the AMO can be attributed to an increase in atmospheric $CO_2$ concentration.

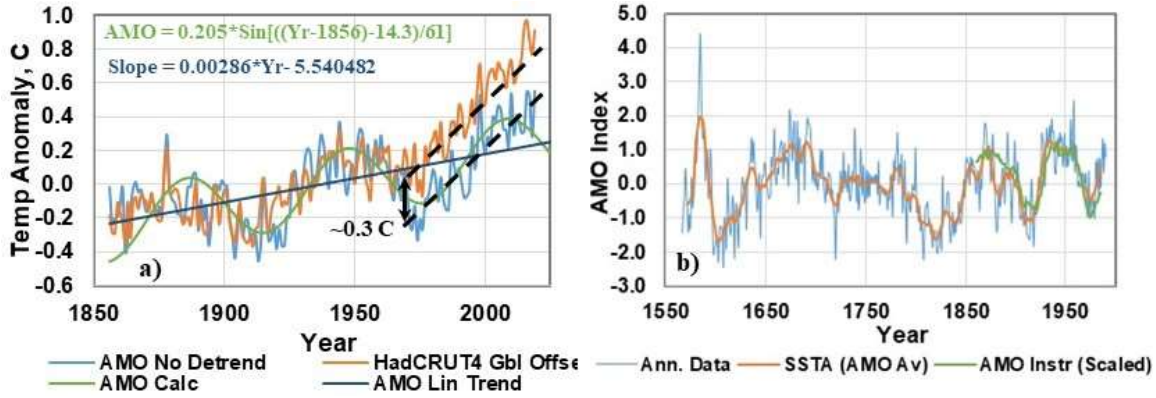


**Figure 11: a) Plots of the HadCRUT4 and AMO temperature anomalies overlapped to show the similarities. Both the long term 60 year oscillation and the shorter term 'fingerprint' details can be seen in both plots. The role of 'adjustments' in the 0.3 C offset since 1970 requires further investigation. b) Tree ring reconstruction of the AMO from 1567.**

There is still an additional part of the recent HadCRUT4 warming that is not included in the AMO signal. This may be explained as a combination of three factors. First there are urban heat islands related to population growth that were not part of the earlier record. Second, the mix of urban and rural weather stations use to create the global record has changed. Third, there are so called 'homogenization' adjustments that have been made to the raw temperature data. These include the 'infilling' of missing data and adjustments to correct for 'bias' related to changes in weather station location and instrumentation. It has been estimated that half of the warming in the 'global record' has been created by such adjustments. This has been considered in more detail by Andrews [2017a, 2017b and 2017c] and by D'Aleo and Watts [2010]. Adjustments to the Australian temperature record have been discussed by Berger and Sherrington [2022].

The role of the AMO in setting the surface air temperature has been misunderstood or ignored for a long time. The first person to claim a measurable warming from an increase in $CO_2$ concentration was Callendar in 1938. He used weather station temperatures up to 1935 that included most of the 1910 to 1940 warming phase of the AMO [Callendar, 1938]. The warming that he observed was from the AMO not $CO_2$. During the 1970s there was a 'global cooling' scare that was based on the cooling phase of the AMO from 1940 to 1970 [McFarlane, 2018, Peterson et al, 2008, Douglas, 1975, Bryson and Dittberner, 1976]. In their 1981 paper Hansen et al chose to ignore the 1940 AMO peak in their analysis of the effects of $CO_2$ on the weather station record [Hansen, 1981]. Similarly Jones et al conveniently overlooked the 1940 AMO peak when they started to ramp up the modern global warming scare in 1986 [Jones et al, 1986]. This is illustrated in Figure 12. The AMO and the periods of record used are shown in Figure 12a. The temperature records used by Callendar, Douglas, Jones et al and Hansen et al are shown in Figures 12b through 12e. The Keeling curve showing the increase in atmospheric $CO_2$ concentration is also shown in Figures 12d and 12e [Keeling, 2022].

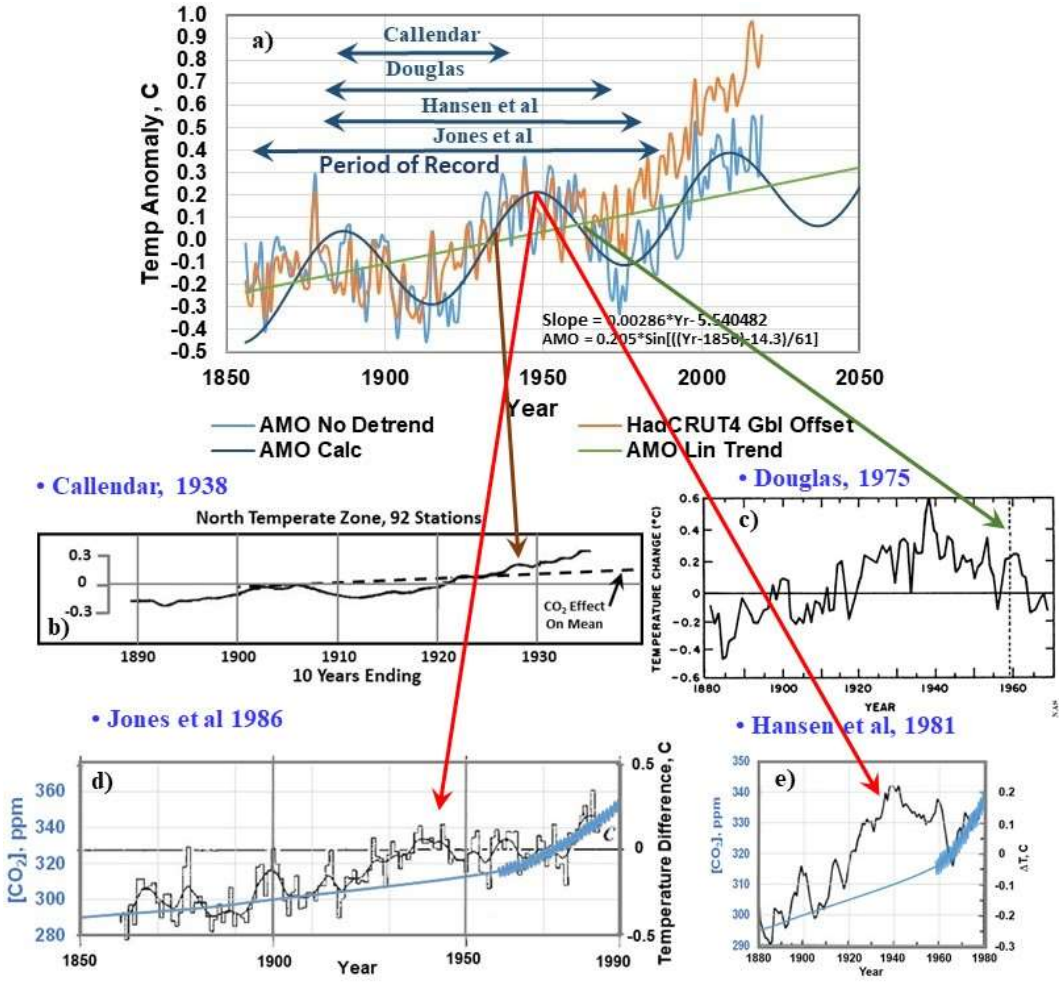


**Figure 12: a) AMO anomaly and HadCRUT4 global temperature anomaly, aligned from 1860 to 1970, b) temperature anomaly for N. temperate stations from Callendar [1938], c) global cooling from Douglas [1975], d) global temperature anomaly from Jones et al, [1986] and e) global temperature anomaly from Hansen et al, [1981]. The changes in $CO_2$ concentration (Keeling curve) are also shown in c and d. The periods of record for the weather station data are also indicated.**

The 'equilibrium' climate modelers have chosen to believe that the 'global mean temperature change' is caused by radiative forcing combined with feedback effects. The equilibrium climate models are 'tuned' so that there is a set of 'radiative forcings' in each model that create the global temperature change record. The models are compared by simulating the increase in 'global temperature' produced by a doubling of the $CO_2$ concentration in the model. This pseudoscientific benchmark is called the climate sensitivity. There are two different ways that the climate sensitivity is determined. First, the $CO_2$ concentration is simply doubled and the model is run to 'equilibrium'. This is called the equilibrium climate sensitivity (ECS). Second, the $CO_2$ concentration is increase gradually, usually by 1% per year. The temperature change at the $CO_2$ doubling point is call the transient climate response (TCR).

In order to 'validate' the climate models, a similar exercise is applied in reverse to the measured 'global mean temperature record'. This may be illustrated by considering the work of Otto et al [2013]. They defined the climate sensitivities as

$$ECS = F_{2x}\Delta T/(\Delta F - \Delta Q) \quad \text{(Eqn. 1a)}$$

$$TCR = F_{2x}\Delta T/\Delta F \quad \text{(Eqn. 1b)}$$

Here, $F_{2x}$ is the radiative forcing produced a doubling of the atmospheric $CO_2$ concentration, set in this case to 3.44 W $m^{-2}$ for a doubling from 'preindustrial levels', 280 to 560 ppm, $\Delta F$ is the change in radiative forcing (W $m^{-2}$), $\Delta T$ (°C) is the change in global mean temperature and $\Delta Q$ is the change in the 'earth system heat content', also given in W $m^{-2}$. The change in temperature is taken from the HadCRUT4 global temperature anomaly and the radiative forcings are taken from the CMIP5/RCP4.5 model ensemble. The change in heat content is dominated by ocean heat uptake. The decadal temperature and forcing estimates from data given by Otto et al are shown in Figures 13a and 13b. The 1910 AMO cycle minimum and the 1940 maximum are indicated. The increase in the downward LWIR flux related to the 'radiative forcing' shown in Figure 13b cannot couple below the ocean surface and cause any measurable change in ocean temperature. Using the data from Figures 13a and 13b combined with estimates of $\Delta Q$ from various sources, Otto et al assume that their net radiative forcing estimates are responsible for the observed heating effects and that the temperature response to the change in LWIR flux is linear. Plots of $\Delta T$ vs ($\Delta F$-$\Delta Q$) and $\Delta T$ vs $\Delta F$ are therefore presumed to be linear with a slope that changes with the value of ECS or TCR. The results generated by Otto et al are shown in Figures 13c and 13d. Using the data for 2000 to 2010, they create an ECS of 2.0 °C with a 5-95% confidence interval of 1.2 to 3.9 °C and a TCS of 1.3 °C with a confidence level of 0.9 to 2.0 °C. The radiative forcings and their time evolution published in the IPCC AR5 climate assessment report [IPCC AR5 WG 1 Chap 8, 2013, Figures 8.17 and 8.18] are shown in Figure 13e and 13f. The radiative forcings for the 'greenhouse gases' are derived from radiative transfer calculations using the HITRAN database or similar data. The various aerosol terms are simply 'tuning knobs' that can be adjusted to give a better fit to the measured temperature data. As shown in Figures 6 and 7 above, the LWIR flux cannot heat the oceans because the penetration depth of the LWIR flux is less than 100 micron. Within the ±30° latitude bands the increase in downward LWIR flux of 2 W $m^{-2}$ from the 140 ppm increase in atmospheric $CO_2$ concentration is dissipated as latent heat by an increase in wind speed of 13 cm $s^{-1}$. The red dotted lines added to Figure 13f indicate the total LWIR forcings and the increase in latent heat flux produced by an increase in wind speed of 13 cm $s^{-1}$. The ECSs for the CMIP5 and CMIP6 model 'ensembles' are shown in Figures 13g and 13h. The CMIP 5 range is from 2.1 to 4.7 °C and the CMIP6 range is from 1.8 to 5.6 °C [IPCC 2013, Chap. 9; Zelinka et al, 2020; Hausfather, 2019]. The correct number is 'too small to measure'. The fundamental error, that the increase in LWIR flux can heat the oceans, can be traced back to Hansen et al [1981].

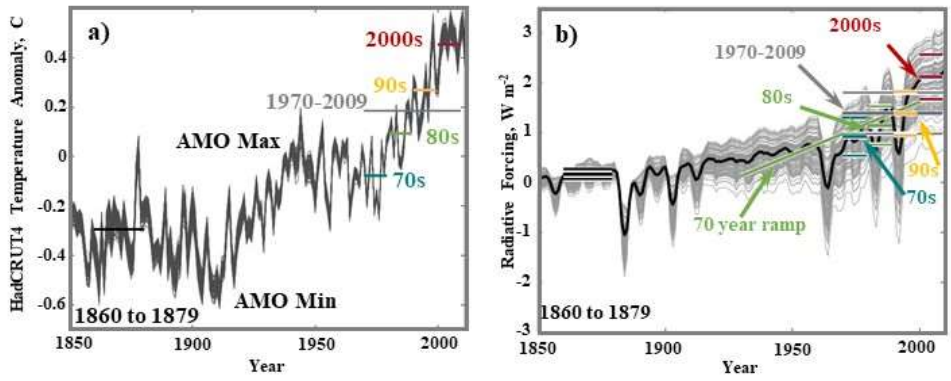
a)
HadCRUT4 Temperature Anomaly, C
2000s
90s
1970-2009
80s
AMO Max
70s
AMO Min
1860 to 1879
Year
b)
Radiative Forcing, W m-2
2000s
1970-2009
80s
90s
70s
70 year ramp
1860 to 1879
Year

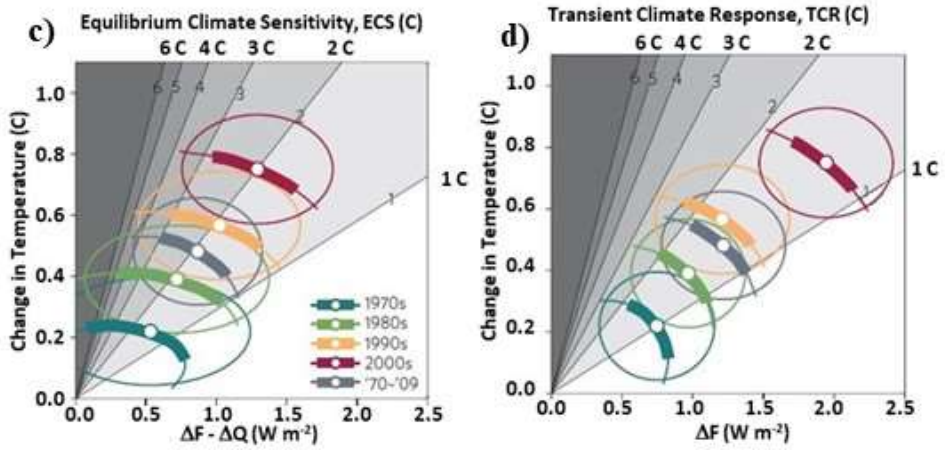
c)
Equilibrium Climate Sensitivity, ECS (C)
6 C 4 C 3 C 2 C
1 C
Change in Temperature (C)
1970s
1980s
1990s
2000s
'70-'09
ΔF - ΔQ (W m-2)
d)
Transient Climate Response, TCR (C)
6 C 4 C 3 C 2 C
1 C
Change in Temperature (C)
ΔF (W m-2)

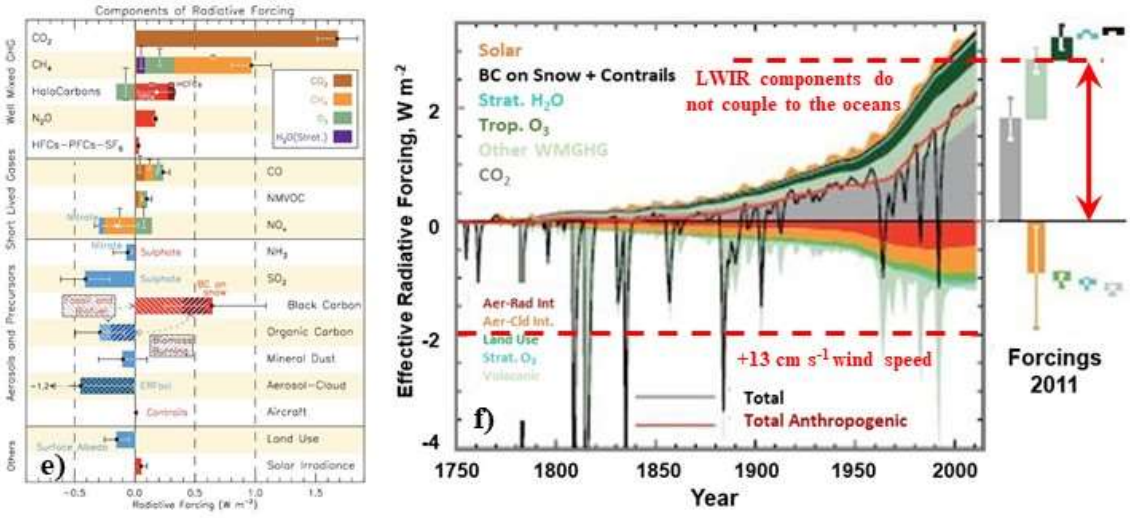
Components of Radiative Forcing
Well Mixed GHG
Short Lived Gases
Aerosols and Precursors
Others
HaloCarbons
CO
NMVOC
Sulphate
Black Carbon
Organic Carbon
Mineral Dust
Aerosol-Cloud
Aircraft
Land Use
Solar Irradiance
e)
Radiative Forcing (W m-2)
Solar
BC on Snow + Contrails
Strat. H2O
Trop. O3
Other WMGHG
CO2
LWIR components do not couple to the oceans
Aer-Rad Int
Aer-Cld Int.
Land Use
Strat. O3
Volcanic
+13 cm s-1 wind speed
Total
Total Anthropogenic
f)
Effective Radiative Forcing, W m-2
Year
Forcings 2011

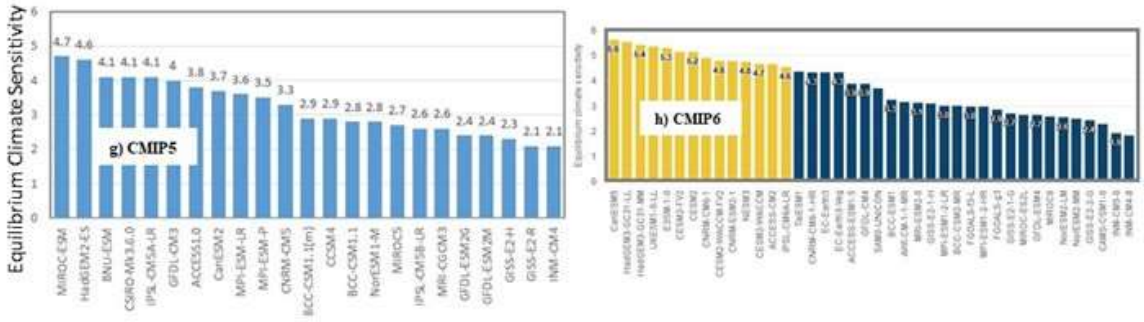


**Figure 13: a) Decadal mean temperature estimates derived from the HadCRUT4 global mean temperature series. b) Decadal mean forcing with standard errors from the CMIP5 /RCP4.5 ensemble. c) Estimates of ECS and d) TCR from Otto et al [2013]. e) Radiative forcings from Figure 8.17 of IPCC AR5 WG1. f) The time dependences of the radiative forcings from f) adapted from figure 8.18 of IPCC AR5. g) The climate sensitivities of various CMIP5 models from IPCC AR5 WG1 Table 9.5 and h) CMIP6 climate sensitivities from Hausfather [2019].**

## There are no 'Human Factors' that can be 'Attributed' to the Warming Found in the Global Mean Temperature Record

The contrived set of radiative forcings used in the climate models to calculate the global mean temperature record is then manipulated to 'attribute' the observed warming to 'human factors'. The 'human factors', mainly the LWIR forcings from the increase in 'greenhouse gases' are turned off and the climate models are rerun with 'natural factors' only. In reality, the most recent warming phase of the AMO and the bias terms are removed from the temperature record. This is illustrated in Figure 14. The global mean temperature change and the results from the CMIP5 model ensemble are shown in Figure 14a. The temperature record is taken from three sources, HadCRUT4, NASA GISS and NCDC. The radiative forcings used in the models are shown above in Figure 13f. The 1940 AMO peak and the 1910 AMO minimum are also indicated. The models are then rerun without the 'human factors'. This is blue line in Figure 14b. The approximate contribution of the AMO, including the warm phases of the oscillation and the linear recovery from the LIA are indicated in Figure 15. The box enclosing the 1910 to 1940 warm phase has simply been copied over to show the recent AMO warming. The rest of the warming may be accounted for by UHI effects, changes to the rural/urban mix of the weather stations used in the global average and the 'homogenization adjustments. Figures 14a and 14b are from a report by Terando et al, *Using information from global climate models to inform policymaking - The role of the U.S. Geological Survey* [2020]. Here the authors have blindly copied the figure from the NCA4, the Fourth USGCRP National Climate Assessment Report [Knutson et al, 2017]. Similar figures with the 'attribution to human factors' were published in NCA3, the Third USGCRP National Climate Assessment Report [Melillo, 2014]. They were also used in the Working Group 1 Report from AR5, the Fifth IPCC Assessment Report. The original work was published by Jones et al, [2013, figure 4]. This is shown in Figure 16.

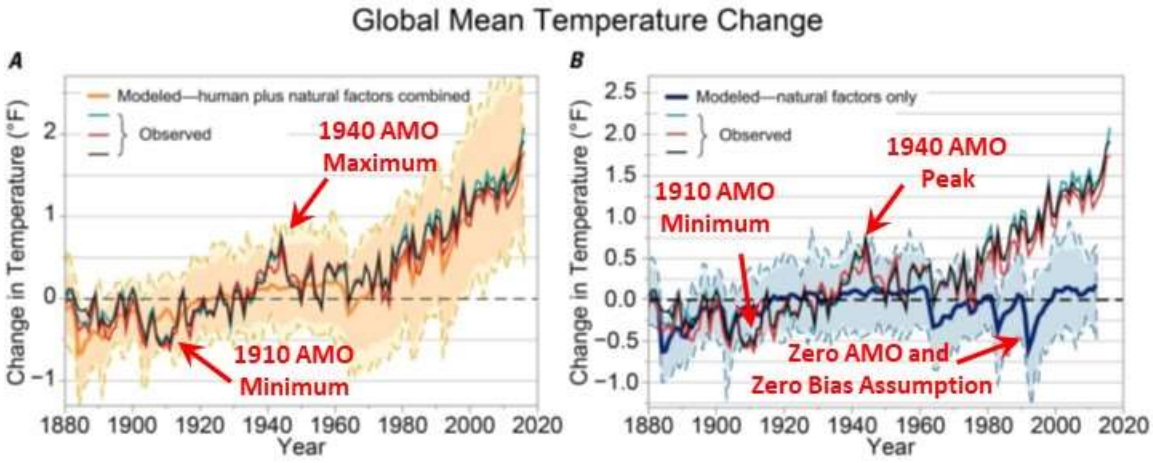


**Figure 14: a) GISTEMP, HadCRUT4.5 and NOAA climate records and the CMIP5 model ensemble results, b) model ensemble with 'anthropogenic forcings' removed. The 1910 AMO minimum and the 1940 AMO peak are indicated.**

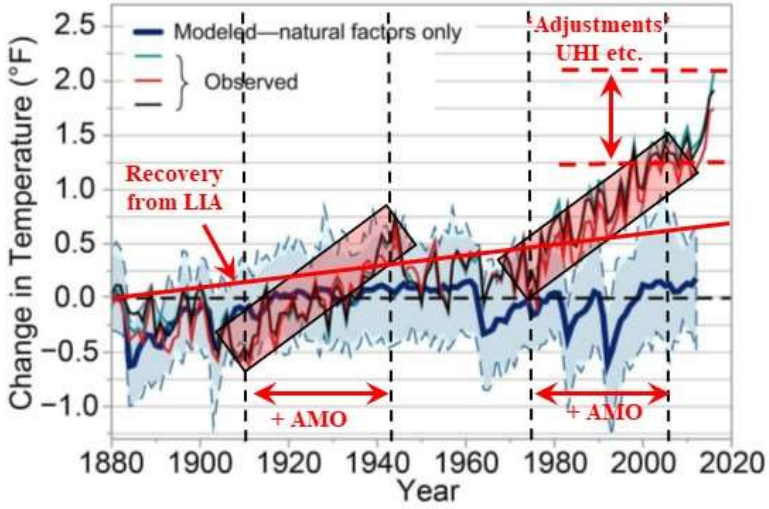


**Figure 15: Figure 14b with the positive phases of the AMO, temperature recovery from the LIA and residual 'adjustments', UHI etc. indicated.**

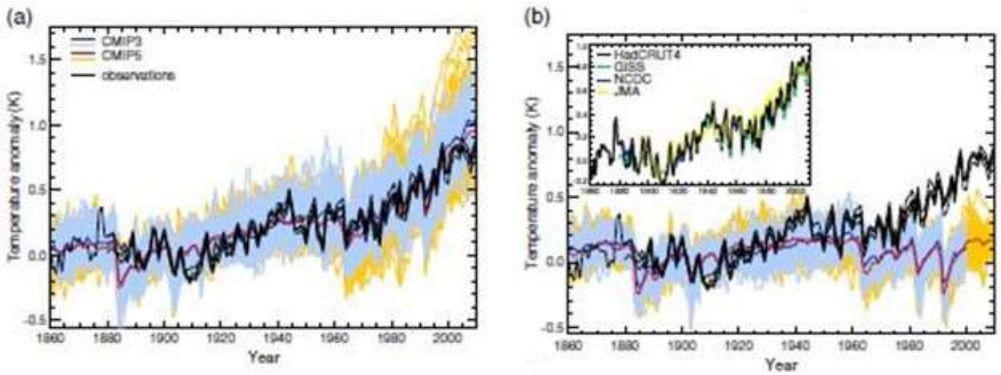

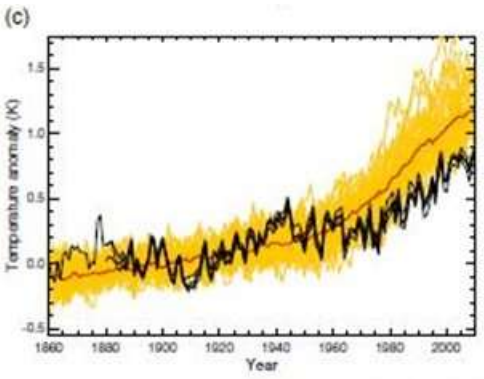


**Figure 16: Figure 4 from Jones et al [2013], a set of contrived radiative forcings is used to 'attribute' the recent warming in the global mean temperature record to human factors'. a) And b) are earlier versions of Figure 14. c) Shows the model output with the 'human factors' included.**

The history of radiative forcing was reviewed by Ramaswamy et al [2019]. This provides a convenient source for the earlier history of climate modeling and radiative forcing. Sets of contrived radiative forcings similar to those shown in Figure 13f have been used by the IPCC to 'attribute' climate change to 'human factors' since it was established in 1988. One of the earliest uses of this approach was by Hansen et al [1981]. Figure 17 shows figures 19 and 15 from Hansen et al [1993] and Figure 18 shows earlier work from figure 5 of Hansen et al [1981].

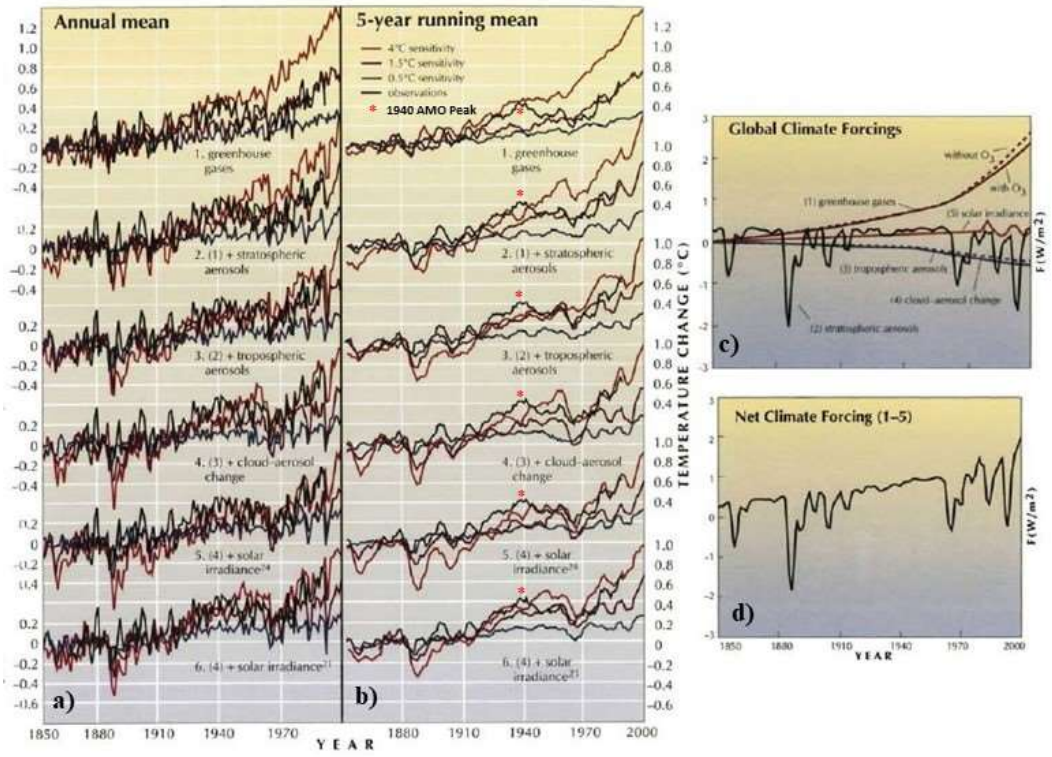


**Figure 17: (Composite from figures 19 and 15 of Hansen et al, 1993) a) and b) simulated global temperature change for 3 climate sensitivities. Successive forcings are added cumulatively. The zero point of observations and model is 1866-1880 mean. c) and d) climate forcings used in the GCM simulations.**

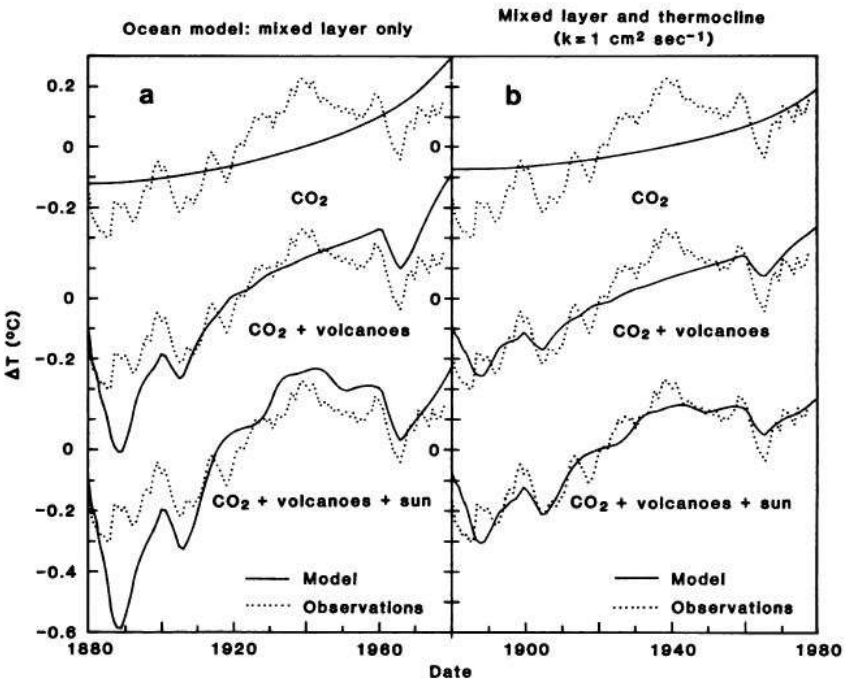


**Figure 18: (Hansen et al, figure 5) Global temperature trend obtained from climate model with sensitivity 2.8 °C for doubled $CO_2$. The results in (a) are based on a 100 m mixed layer ocean for heat capacity; those in (b) include diffusion of heat into the thermocline to 1000 m.**

## There can be no Increase in Extreme Weather Events 'Attributable' to $CO_2$.

The same set of contrived radiative forcings used to create the global mean temperature record is then used to make fraudulent claims that 'human factors' are causing increases in 'extreme weather'. One of the more egregious examples of this is the annual supplement to the Bulletin of the American Meteorological Society 'Explaining Extreme Events of [Year] from a Climate Perspective' [Herring et al, 2022]. The series has been published annually since 2012. The BAMS publication guidelines clearly state:

> 'Each paper will start with a 30 word capsule summary that includes, if possible, how anthropogenic climate change contributed to the magnitude and/or likelihood of the event'.

The climate sensitivities created in CMIP5 and CMIP6 model ensembles and other in climate models are used without question to 'explain' the observed 'extreme weather events' for the year of interest. Natural climate changes related for example to ocean oscillations and blocking high pressure systems have to be 'enhanced' by the pseudoscience of radiative forcings.

An important source of heat in the lower troposphere is air compression. This has been largely ignored by the 'equilibrium' climate modelers. As dry air descends to lower altitudes, the lapse rate is 9.8 K $km^{-1}$. There are two main effects. The first is heating by downslope winds and the second is the heating produced by the downward flow of air within a high pressure 'dome'. These processes can produce temperature changes of 10 °C or more over a few days or less. Downslope winds are well known in many regions or the world and there are many different names for the

same effect. In S. California they are Santa Ana Winds. In N. California they are diablo winds. In the Rocky Mountains they are chinook ('snow eating') winds. In the Alps they are föhn winds. There is no connection between these downslope wind events and any increase in atmospheric $CO_2$ concentration. Once the necessary weather pattern is established, the hot, dry winds will finish drying out the vegetation very quickly and any ignition source will start a wildfire. The Santa Ana winds in S. California are a good example of this. The air circulation within a high pressure system produces a downward air flow because of the Coriolis Effect. This provides a natural heat source for these systems. A stationary or blocking high pressure system can result in significant warming over a period of several days. Further details of these heating effects are provided by Clark and Rörsch [2023].

**Climate Models Have No Predictive Capabilities Because of Lorenz Instabilities**

In 1963, Lorenz was evaluating a simple model of three coupled non-linear equations that described two dimensional convective flow. He discovered that the solutions to these equations were unstable and sensitive to small changes in the starting variables [Lorenz, 1963]. This is illustrated in Figure 19. He later established that weather forecasting predictions were limited to approximately 12 days ahead before the model instabilities became dominant [Lorenz, 1973].

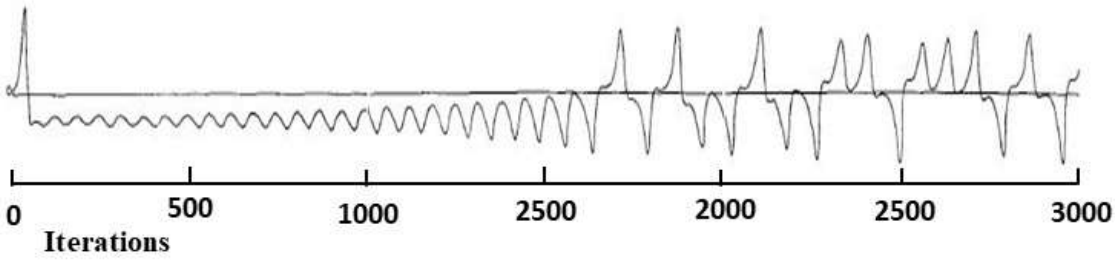


**Figure 19: Lorenz instabilities for 3 coupled partial differential equations, from Lorenz, 1963.**

The large scale climate models used today require the solution of a very large number of coupled non-linear equations. There is no reason to expect such models to have any predictive capabilities. They are inherently unstable and have to be 'tuned' to give the desired results. In fact, they can be 'tuned' to give any desired result. All of the CMIP5 and CMI6 climate models shown in Figures 13g and 13h have been tuned based on the pseudoscience of radiative forcing to create the global surface temperature anomaly. The fact that all of these models have a similar climate sensitivity to $CO_2$ is clear evidence of the climate fraud. A realistic climate model should not show any measurable 'climate sensitivity' to $CO_2$.

**References**

AMO (2022), [https://www.esrl.noaa.gov/psd/data/correlation/amon.us.long.mean.data]

Akasofu, S.-I. (2010), "On the recovery from the Little Ice Age" *Natural Science* **2**(11) pp. 1211-1224. [http://dx.doi.org/10.4236/ns.2010.211149]

Andrews, R. (2017a), "Adjusting Measurements to Match the Models – Part 3: Lower Troposphere Satellite Temperatures" *Energy Matters* Sept 14. [http://euanmearns.com/adjusting-measurements-to-match-the-models-part-3-lower-troposphere-satellite-temperatures/#more-19464]

Andrews, R. (2017b), "Making the Measurements Match the Models – Part 2: Sea Surface Temperatures" *Energy Matters* Aug 2. [http://euanmearns.com/making-the-measurements-match-the-models-part-2-sea-surface-temperatures/]

Andrews, R. (2017c), "Adjusting Measurements to Match the Models – Part 1: Surface Air Temperatures" Energy Matters July 27. [http://euanmearns.com/adjusting-measurements-to-match-the-models-part-1-surface-air-temperatures/]

Arrhenius, S. (1896), "On the influence of carbonic acid in the air upon the temperature of the ground" *Philos. Trans.* **41** pp. 237-276. [https://doi.org/10.1080/14786449608620846]

Berger, T. and G. Sherrington, (2022), "Uncertainty of Measurement of Routine Temperatures–Part Three" WUWT Oct 14 https://wattsupwiththat.com/2022/10/14/uncertainty-of-measurement-of-routine-temperatures-part-iii/

Bryson, R. A. and G. J. Dittberner (1976), "A non-equilibrium model of hemispheric mean surface temperature" *J. Atmos. Sci.* **33**(11) pp. 2094-2106. [https://journals.ametsoc.org/view/journals/atsc/33/11/1520-0469_1976_033_2094_anemoh_2_0_co_2.xml]

Callendar, G. S. (1938), "The artificial production of carbon dioxide and its influence on temperature" *J. Roy. Met. Soc.* **64** pp. 223-240. [https://doi.org/10.1002/qj.49706427503; availabe at: http://www.met.reading.ac.uk/~ed/callendar_1938.pdf]

Clark, R. (2013), "A dynamic, coupled thermal reservoir approach to atmospheric energy transfer Part I: Concepts" *Energy and Environment* **24**(3, 4) pp. 319-340. [https://doi.org/10.1260/0958-305X.24.3-4.319]

"A dynamic, coupled thermal reservoir approach to atmospheric energy transfer Part II: Applications" *Energy and Environment* **24**(3, 4) pp. 341-359. [https://doi.org/10.1260/0958-305X.24.3-4.341]

Clark, R. and A, Rörsch (2023), *Finding simplicity in a complex world*, Amazon (In Press).

D'Aleo, J. and A. Watts (Aug. 27, 2010) "Surface temperature records: policy driven deception? [http://scienceandpublicpolicy.org/images/stories/papers/originals/surface_temp.pdf] (Link not working) Available at: [https://venturaphotonics.com/files/6.0_D'Aaleo.Watts.Surface_temp.SPPC%202010.pdf]

Douglas, J. H. (March 1, 1975) "Climate change: chilling possibilities" *Science News* **107** pp. 138-140. [https://www.sciencenews.org/wp-content/uploads/2008/10/8983.pdf]

Feldman D.R., K. N. Liou, R. L. Shia and Y. L. Yung (2008), "On the information content of the thermal IR cooling rate profile from satellite instrument measurements" *J. Geophys. Res.* **113** D1118 pp. 1-14. [https://doi.org/10.1029/2007JD009041]

Fourier, J.-B.-J. (1824), "Remarques générales sur les températures du globe terrestre et des espaces planétaires" *Annales de Chimie et de Physique* **27**, pp. 136–167.

[https://gallica.bnf.fr/ark:/12148/bpt6k65708960/f142.image#] English translation: [http://fourier1824.geologist-1011.mobi/]

Gibert, F.; J. Cuesta, J.-I. Yano, N. Arnault and P. H. Flamant (2007), "On the Correlation between Convective Plume Updrafts and Downdrafts, Lidar Reflectivity and Depolarization Ratio" *Boundary Layer Meteorology* **5** pp. 553-573. [https://doi.org/10.1007/s10546-007-9205-6]

Gray, S. T.; L. J. Graumlich, J. L. Betancourt and G. T. Pederson (2004) "A tree-ring based reconstruction of the Atlantic Multi-decadal Oscillation since 1567 A.D." *Geophys. Res. Letts*, **31** L12205, pp. 1-4. [https://doi.org/10.1029/2004GL019932]

Gray, S. T., et al. (2004), *Atlantic Multi-decadal Oscillation (AMO) Index Reconstruction*, IGBP PAGES/World Data, Center for Paleoclimatology, Data Contribution Series #2004-062, NOAA/NGDC Paleoclimatology Program, Boulder CO, USA. [https://www.ncei.noaa.gov/pub/data/paleo/treering/reconstructions/amo-gray2004.txt]

HadCRUT4, 2022, https://www.metoffice.gov.uk/hadobs/hadcrut4/data/current/time_series/HadCRUT.4.6.0.0.annual_ns_avg.txt

Hale, G. M. and M. R. Querry (1973), "Optical constants of water in the 200 nm to 200 µm wavelength region" *Applied Optics* **12**(3) pp. 555-563. [https://doi.org/10.1364/AO.12.000555]

Hansen, J. et al., (45 authors), (2005), "Efficacy of climate forcings" *J. Geophys Research* **110** D18104 pp.1-45. [https://pubs.giss.nasa.gov/docs/2005/2005_Hansen_ha01110v.pdf]

Hansen, J.; D. Johnson, A. Lacis, S. Lebedeff, P. Lee, D. Rind and G. Russell (1981), "Climate impact of increasing carbon dioxide" *Science* **213** pp. 957-956. [https://pubs.giss.nasa.gov/docs/1981/1981_Hansen_ha04600x.pdf]

Hansen, J.; A. Lacis, R. Ruedy M. Sato and H. Wilson (1993), "How sensitive is the world's climate?" *National Geographic Research and Exploration* **9**(2) pp. 142-158. [https://pubs.giss.nasa.gov/docs/1993/1993_Hansen_ha02800o.pdf]

Harde, H. (2017), "Radiation Transfer Calculations and Assessment of Global Warming by $CO_2$" *Int. J. Atmos. Sci.* 9251034 pp. 1-30. [https://doi.org/10.1155/2017/9251034]

Hausfather, Z. (2019), "CMIP6: The next generation of climate models explained" *Carbon Brief* [https://www.carbonbrief.org/cmip6-the-next-generation-of-climate-models-explained]

Herring, S. C.; N. Christidis, A. Hoell and P. A. Stott (2022), "Explaining Extreme Events of 2020 from a Climate Perspective" *Bull. Amer. Meteor. Soc.* **101** (1), pp. S1–S128, [https://doi.org/10.1175/BAMS-ExplainingExtremeEvents2020.1] (and prior years in this series)

Iacono, M. J., J. S. Delamere, E. J. Mlawer, M. W. Shephard, S. A. Clough, and W. D. Collins (2008), "Radiative forcing by long-lived greenhouse gases: Calculations with the AER radiative transfer models" *J. Geophys. Res.* **113**, D13103 pp. 1-8. [https://doi.org/10.1029/2008JD009944]

IPCC, *Climate Change 2021: The Physical Science Basis*. *Contribution of Working Group I to the Sixth Assessment Report of the Intergovernmental Panel on Climate Change* [Masson-Delmotte, V.; P. Zhai, A. Pirani, S.L. Connors, C. Péan, S. Berger, N. Caud, Y. Chen, L. Goldfarb, M.I. Gomis, M. Huang, K. Leitzell, E. Lonnoy, J.B.R. Matthews, T.K. Maycock, T.

Waterfield, O. Yelekçi, R. Yu, and B. Zhou (eds.)]. Cambridge University Press, Cambridge, United Kingdom and New York, NY, USA. (2021). In Press. [doi:10.1017/9781009157896, https://www.ipcc.ch/report/ar6/wg1/]

IPCC, *Climate Change 2013: The Physical Science Basis. Contribution of Working Group I to the Fifth Assessment Report of the Intergovernmental Panel on Climate Change* [Stocker, T.F., D. Qin, G.-K. Plattner, M. Tignor, S.K. Allen, J. Boschung, A. Nauels, Y. Xia, V. Bex and P.M. Midgley (eds.)]. Cambridge University Press, Cambridge, United Kingdom and New York, NY, USA, (2014)1535 pp. ISBN 9781107661820. [https://www.ipcc.ch/report/ar5/wg1/]

Jones, G. S.; P. A. Stott and N. Christidis (2013), "Attribution of observed historical near surface temperature variations to anthropogenic and natural causes using CMIP5 simulations" *J. Geophys. Res. Atmos.* **118**(10) pp. 4001-4024. [https://doi.org/10.1002/jgrd.50239]

Jones, P. D.; T. M. Wigley and P. B Wright (1986), "Global temperature variations between 1861 and 1984" *Nature* **323**(31) pp. 430-434. [https://www.nature.com/articles/322430a0]

Keeling (2022), *The Keeling Curve*. [https://scripps.ucsd.edu/programs/keelingcurve/]

Knutson, T.; J.P. Kossin, C. Mears, J. Perlwitz and M.F. Wehner (2017), "Detection and attribution of climate change" In: *Climate Science Special Report: Fourth National Climate Assessment, Volume I*, Wuebbles, D.J., D.W. Fahey, K.A. Hibbard, D.J. Dokken, B.C. Stewart, and T.K. Maycock (eds.). U.S. Global Change Research Program, Washington, DC, USA, pp. 114-132, doi: [https://doi.org/10.7930/J0J964J6]

Knutti, R. and G. C. Hegerl (2008), "The equilibrium sensitivity of the Earth's temperature to radiation changes" *Nature Geoscience* **1** pp. 735-743. [https://www.nature.com/articles/ngeo337]

Lettau, H. H. and B. Davidson (1957), Exploring the Atmosphere's First Mile. Proceedings of the Great Plains Turbulence Field Program, 1 August to 8 September 1953 Volume II, Site Description and Data Tabulation, Oxford, Pergamon Press.

Available at:
[https://books.google.com/books?hl=en&lr=&id=5bcJAQAAIAAJ&oi=fnd&pg=PA377&dq=Lettau,+H.H.+and+B.+Davidson,+Exploring+the+atmosphere%E2%80%99s+first+mile.+Oxford:+Pergamon+Press,+1957.&ots=N0vbpjURx3&sig=sSTz9EMWpwi0XysXHTcWcLNxWv0#v=onepage&q&f=false]

Lorenz, E. N. (1973), "On the Existence of Extended Range Predictability" *J. Applied Meteorology and Climatology* **12**(3) pp. 543-546.
[https://journals.ametsoc.org/view/journals/apme/12/3/1520-0450_1973_012_0543_oteoer_2_0_co_2.xml?tab_body=fulltext-display]

Lorenz, E.N. (1963), "Deterministic nonperiodic flow" *Journal of the Atmospheric Sciences* **20**(2) pp. 130-141. [https://doi.org/10.1175/1520-0469(1963)020<0130:DNF>2.0.CO;2]

Manabe, S. and R. T. Wetherald (1975), "The effects of doubling the $CO_2$ concentration in the climate of a general circulation model" *J. Atmos. Sci.* **32**(1) pp. 3-15.
[https://journals.ametsoc.org/view/journals/atsc/32/1/1520-0469_1975_032_0003_teodtc_2_0_co_2.xml?tab_body=pdf]

Manabe, S. and R. T. Wetherald (1967), "Thermal equilibrium of the atmosphere with a given distribution of relative humidity" *J. Atmos. Sci.* **24** pp. 241-249. [http://www.gfdl.noaa.gov/bibliography/related_files/sm6701.pdf]

McFarlane, F. (2018), "The 1970s Global Cooling Consensus was not a Myth" Watts Up with That, 11.19.2018 [https://wattsupwiththat.com/2018/11/19/the-1970s-global-cooling-consensus-was-not-a-myth/]

Melillo, J. M., T. C. Richmond, and G. W. Yohe, eds., (2014) *Climate Change Impacts in the United States: The Third National Climate Assessment*. U.S. Global Change Research Program, 841 pp.

[https://www.nrc.gov/docs/ML1412/ML14129A233.pdf; on line https://nca2014.globalchange.gov/]

MODTRAN (2021), [http://forecast.uchicago.edu/Projects/modtran.orig.html]

Oke T. R. (2006), *Initial guidance to obtain representative meteorological observations at urban sites* WMO/TD-No. 1250, World Meteorological Association.

[https://www.researchgate.net/publication/265347633_Initial_guidance_to_obtain_representative_meteorological_observations_at_urban_sites]

Otto, A., F. E. L. Otto, O. Boucher, J. Church, G. Hegerl, P. M. Forster, N. P. Gillett, J. Gregory, G. C. Johnson, R Knutti, N. Lewis, U. Lohmann, J. Marotzke, G. Myhre, D. Shindell, B. Stevens and M. R. Allen (2013), "Energy budget constraints on climate response" *Nature Geoscience*, **6** (6). pp. 415 - 416. ISSN 1752-0894. [http://eprints.whiterose.ac.uk/76064/7/ngeo1836(1)_with_coversheet.pdf]

Otto Ibid, Supplementary Material. [https://static-content.springer.com/esm/art%3A10.1038%2Fngeo1836/MediaObjects/41561_2013_BFngeo1836_MOESM299_ESM.pdf]

Peterson, T. C.; W. M. Connolley and J. Fleck, (2008) "The myth of the 1970's global cooling consensus" *Bull. Amer. Meteor. Soc.*, **86** pp. 1325-1337. [https://doi.org/10.1175/2008BAMS2370.1]

Ramanathan, V. (1975), "Greenhouse effect due to chlorofluorocarbons: Climatic implications" *Science* **190**, pp. 50-52 [https://www.science.org/doi/abs/10.1126/science.190.4209.50]

Ramaswamy, V.; W. Collins, J. Haywood, J. Lean, N. Mahowald, G. Myhre, V. Naik, K. P. Shine, B. Soden, G. Stenchikov and T. Storelvmo (2019), "Radiative Forcing of Climate: The Historical Evolution of the Radiative Forcing Concept, the Forcing Agents and their Quantification, and Applications" *Meteorological Monographs* Volume **59** Chapter 14. [https://doi.org/10.1175/AMSMONOGRAPHS-D-19-0001.1]

Terando, A. D. Reidmiller, S. W. Hostetler, J. S. Littell, T. D. Beard, Jr., S. R. Weiskopf, J. Belnap, G. S. Plumlee (2020), "Using information from global climate models to inform policymaking—The role of the U.S. Geological Survey" *U.S. Geological Survey Open-File Report 2020–1058*, 25 pp. [https://doi.org/10.3133/ofr20201058 ]

Wang, W. C. and G. A. Domoto (1974), "The radiative effect of aerosols on the earth's atmosphere" *J. Appl. Meteorology* **13**(5) pp. 521-534. [https://doi.org/10.1175/1520-0450(1974)013<0521:TREOAI>2.0.CO;2]

Wang, W. C.; Y. L. Yung, A. A. Lacis, T. Mo and J. E. Hansen (1976), "Greenhouse effects due to man-made perturbations of trace gases" *Science* **194** pp. 685-690. [https://pubs.giss.nasa.gov/docs/1976/1976_Wang_wa07100z.pdf]

Wijngaarden, W. A. van and W. Happer (2022), "IR Forcing by Greenhouse Gases" $CO_2$ Coalition publication 6/10/22, [https://co2coalition.org/wp-content/uploads/2022/03/Infrared-Forcing-by-Greenhouse-Gases-2019-Revised-3-7-2022.pdf]

WRCC (2022), [https://wrcc.dri.edu/sod/arch/hbF.html]

Yu, L., X. Jin, and R.A. Weller (Jan. 2008), "*Multidecade global flux datasets from the objectively analyzed air-sea fluxes (OAFlux) project: latent and sensible heat fluxes, ocean evaporation, and related surface meteorological variables*" OAFlux project technical report OA-2008-01. [https://rda.ucar.edu/datasets/ds260.1/docs/OAFlux_TechReport_3rd_release.pdf]

Zelinka, M. D.; T. A. Myers, D. T. McCoy, S. Po-Chedley, P. M. Caldwell, P. Ceppi, S. A. Klein and K. E. Taylor, "Causes of Higher Climate Sensitivity in CMIP6 Models" *Geophysical Research Letters* **47**, e2019GL085782 pp1-12 (2020). [https://agupubs.onlinelibrary.wiley.com/doi/pdf/10.1029/2019GL085782]